IEEE Access
Multidisciplinary | Rapid Review | Open Access Journal

Received November 6, 2020, accepted November 18, 2020, date of publication November 24, 2020,
date of current version December 8, 2020.

Digital Object Identifier 10.1109/ACCESS.2020.3040001

Analysis of Sensor-Based Real-Time Balancing of Humanoid Robots on Inclined Surfaces

SUNANDAN DUTTA[1,2], TAPAS KUMAR MAITI[2], (Member, IEEE), MITIKO MIURA-MATTAUSCH[2], (Fellow, IEEE), YOSHIHIRO OCHI[2], NAOTO YORINO[1], (Senior Member, IEEE), AND HANS JÜRGEN MATTAUSCH[2], (Senior Member, IEEE)

[1]Graduate School of Engineering, Hiroshima University, Higashi-Hiroshima 739-8527, Japan
[2]HiSIM Research Center, Hiroshima University, Higashi-Hiroshima 739-8530, Japan

Corresponding author: Sunandan Dutta (sunandan-dutta@hiroshima-u.ac.jp)

This work was supported in part by the TAOYAKA Leading Graduate Education Program, Hiroshima University, Japan.

ABSTRACT An experimental and theoretical study of real-time robot balancing on inclined surfaces with electrical feedback circuitry is presented. Force sensors are experimentally shown to extend the sustainability of a stable robot posture beyond a critical surface inclination. For this purpose, the inclination feedback from the force sensors is used to adjust the robot's ankle-pitch-motor angle above the critical inclination, thus enabling the maintenance of a stable robot posture. Further, the Inverted Pendulum Model (IPM) (Hemami and Golliday, 1977, Hemami *et al.*, 1973, and McGhee and Kuhner, 1969) is extended to the case of inclined surfaces. Through application of this extended IPM it is demonstrated, that simultaneous use of gyro-sensor data can minimize the necessary initial adjustment of the motor angle for controlled robot-body rotation, which additionally has the positive effect of reducing possible overshoots of the motor's rotation angle during feedback. Consequently, the reported feedback control improves the robot-body stability on inclined surfaces. Efficient implementation of the developed control scheme into an existing robot's electrical system is proposed.

INDEX TERMS Balanced walking control, force sensor, gyro sensor, humanoid robot, servo motor.

I. INTRODUCTION

Robots have been developed and utilized for reducing the necessity of direct human labor in various sectors of the society. Environments like medical supervision for highly infectious diseases, disaster rescue, internal power-plant investigation or space exploration are suitable for appropriately specialized robots [1]–[6]. In particular, humanoid robots are desirable for directly supporting many needs related to the human existence, and their deployment is now planned in various fields of the human society, where dynamical walking with high degrees of freedom similar to human beings becomes necessary. In recent times, the robotics community has demonstrated large progress in developing such highly-intelligent humanoid robots for usage in various adverse environments [7]–[10].

Robot-walking control on a specific surface requires accurate detection of the surface-profile information [11]–[18]. Most of the development in this field extensively utilizes specific measured terrain information to stabilize the walking pattern [14]–[15]. Previously developed robots often rely on surface-profile information, according to which they make walking-pattern changes by controlling their joint-motor angles for overcoming or avoiding obstacles. Typically, the environment information is collected by cameras or similar vision-based sensors [19]–[20]. Therefore, the case of a ''blind'' humanoid robot, without any camera to sense the environment, can be a worst-case scenario for robot-stability control [16]–[18]. In such a case, the surface interaction with force/torque sensors, integrated under the robot feet [16], becomes an important information source for assuring robustness and stability of the robot.

Published robot-control methods for ''blind'' robots have focused on robot-walking analysis [21]–[24]. Model-based control such as the Zero Moment Point (ZMP) control was introduced to analyze and improve the dynamic walking by applying ZMP-position adjustments [25], [26], and is utilized in many industrial robots and industrial

The associate editor coordinating the review of this manuscript and approving it for publication was Okyay Kaynak.

humanoids like the Honda Humanoid Robot [27] or the HRP series of AIST [28], [29]. However, unlike well-solved control problems as those for robot hands or manipulators [30], [31], the development of robust and agile humanoid-robot control has not yet reached practical implementation. Recently, control systems based on Machine Learning (ML) algorithms, such as supervised-learning algorithms [32]–[34] and reinforcement-learning algorithms [35], [36], are applied in model-based systems for biped-stability control [21], [23], [26], [37]–[39] to achieve better walking dynamics of humanoid robots. A major implementation problem for such software-based control methods in light-weight robots is the required hardware complexity and the high necessary processing power. Consequently, it is difficult to implement such Artificial Intelligence (AI) software into a commercial low-cost mass-produced open-source hardware platform and then integrate such a platform into a light-weight robot. Even in case of successful integration, the weight of the robot and its power consumption will significantly increase, making the overall development quite inefficient, both from the mechanical and the electrical point of view. In summary, the balancing of the light humanoid robots, cannot be efficiently realized using such previously proposed dynamic walking-pattern control. Further, the balancing of light-weight robots on an inclined surface is more difficult than that of a heavy-weight robot [15]–[18]. Under observation of the scalability rules [40], very few investigations on balancing light-weight humanoid robots on an inclined surface have been reported [41], [42]. Tamura and Kawamura [41] proposed a stability control for light-weight humanoid robots without calculating the robot's ZMP, thus avoiding the calculation overhead and also the effect of ZMP-calculation-induced joint-angle-determination noise during robot stabilization on inclined surfaces. Implementation of the proposed scheme showed, that the robot can only step over an object (unevenness) of 0.5 cm height, which is quite inadequate with respect to the more realistic uneven surfaces and obstacles. Moreover, the control scheme of [41] was not applied to any inclined surface (upslope or downslope). Yi *et al.* [42] proposed a ZMP-based on-line-learning system, where the robot calculated the surface inclination while walking and adjusted the joint angles for stable posture of the body's Center of Mass (COM). Though implemented for an uneven surface with 6% finite height change, the inclined-surface effects on static stability and walking dynamics of the robot are not discussed. The capability of stable walking on an inclined surface, while having a limited motor-torque rating, slow control-update rates and relatively high sensor noise, is a general challenging problem for the light-weight robots.

Our investigation focusses on the development of humanoid-robot-stability control, which is valid even for light-weight robots. The novel contributions of the reported work include:

- Force-sensor attachment to heel and toe of the robot feet, which enables force-difference measurements between toe and heel sensors as a function of surface inclination. Based on these differences, a critical surface inclination can be determined, below which no sensor-based motor control (force or gyro sensors) is required. (see Section II)
- Inverted Pendulum Model (IPM) [43], [45] extension to inclined surfaces by including the impact of gravity-force-direction changes relative to the robot body. (see Section III-A and B)
- Based on this extended IPM, an ankle-pitch-motor control system with force-sensor feedback is proposed, which is easy to implement in an open hardware platform with minimal power overhead. (see Section III-C)
- Compared to the conventional ZMP control [46], the necessity of ZMP determination can be eliminated due to the force sensors, reducing calculation overhead and noise. As the ankle-pitch motor plays an important role in posture stabilization [43], [44], [47], only ankle-pitch-motor control, based on toe- and heel-force differences, is initially applied. This further reduces calculation complexity in comparison to the conventional inverse-kinematics-based approach for all joint-angles [25]. (see Sections III-C and IV)
- For relatively large inclinations, a gyro-sensor-based hip-motor control is introduced in addition to the force-sensor-based ankle-motor control. (see Sections III-C and IV)
- A particular focus is the stability improvement through real-time feedback of the sensor data within the control system. With the extended IPM it becomes possible to predict the critical surface inclinations for robot stability. Based on the developed control systems, robot stability can thus be increased at higher surface inclinations. (see Sections IV and V)

The section structure of this paper is outlined as follows. Section II explains the experiments carried out with the humanoid robot on inclined surfaces and the measured results. In Section III, the developed robot model, incorporating the sensor data, is presented through an extension of the IPM. The hardware implementation of the developed control method is discussed in Section IV. Section V concludes the paper.

II. EXPERIMENTS FOR ROBOT-BALANCING ANALYSIS

The used commercial KONDO robot [48] with height of 0.4 m (see Table 1 for the physical parameters of the robot) allows us to implement our investigation and is therefore suitable for measuring the desired robot-balancing features. The robot walks by itself downslope on a smooth surface under the control of 17 motors, as illustrated in Fig. 1. Among these 17 motors, 3 motors for each leg are used to realize the basic walking action of the robot. The locations of these 3 motors (M_A = Ankle-pitch motor, M_K = Knee Motor and M_H = Hip-pitch motor) on each leg are depicted in the schematic of Fig. 2.

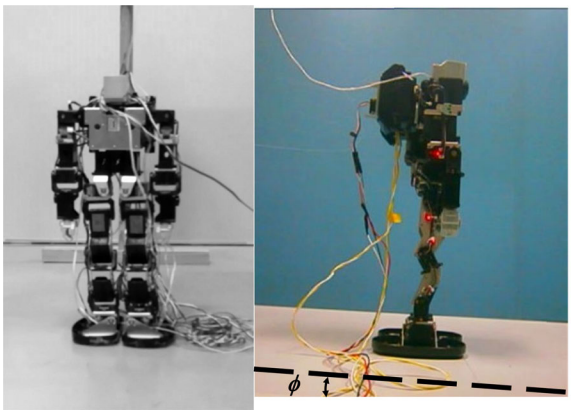

FIGURE 1. Experimental setup for the robot-walking experiments on a surface with inclination ϕ.

TABLE 1. KONDO KHR-3HV robot physical parameters.

Parameter	Unit	Amount
Height	m	0.4
Length of foot	m	0.12
Mass[+]	kg	1.5
Degrees of Freedom*	-	17

[+]Robot mass is measured after integrating all sensors and the controller in the backpack.

*The degrees of freedom for the robot are given by the number of motors used in the robot. However, for walking analysis and balancing, we considered just the three motors in each robot leg. The motors are shown in the Fig.2 as M_A for ankle-pitch motor, M_K for knee motor and M_H for the hip-pitch motor.

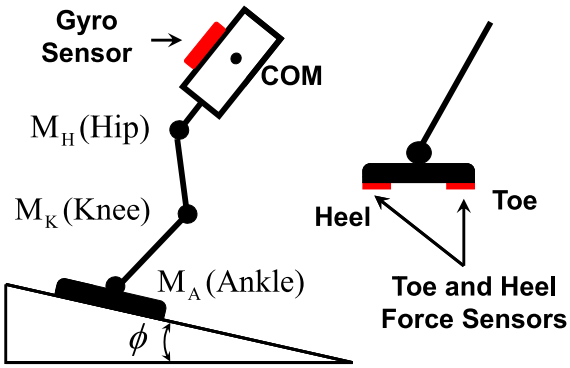

FIGURE 2. Schematic representation of the experimental setup for the robot-walking experiments, showing the sensor locations below the robot feet and on the robot body.

A. EXPERIMENTAL SETUP

Two force sensors (toe and heel) are attached on the bottom of each foot, as indicated in Fig. 2. To analyze the balancing mechanism of the robot, a smooth surface is inclined by an angle ϕ and the force on each sensor is measured. The inclination of the surface is gradually increased from 0° to around 10°. Measurements with the setup shown in Fig. 2 are performed for three situations:

1. The sensor forces are recorded, when the robot is standing on the inclined surface without motor control.

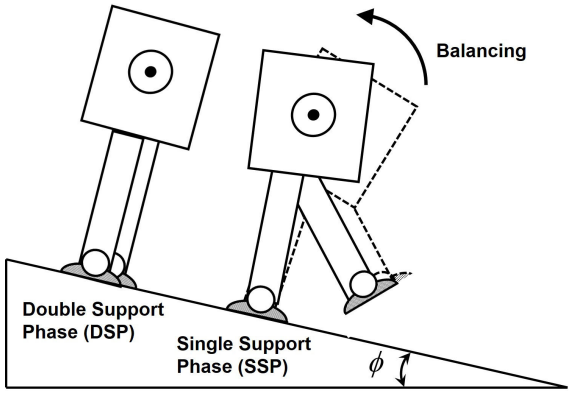

FIGURE 3. Schematic indication of the characteristics of the Single Support Phase (SSP) and the Double Support Phase (DSP).

2. The ankle-pitch motor (M_A) is rotated in order to allow the robot to sustain a stable posture, if the robot becomes unstable due to an increased surface inclination.
3. The hip-pitch motor (M_H) is rotated according to the gyro-sensor information, to further extend the surface-inclination range with robot-posture stability.

Our focus is given on the balancing mechanism of a humanoid robot on inclined surfaces. For this purpose, we perform experiments for a robot with relatively slippery feet on a slippery surface, to enhance the robot's instability sensitivity without additional active robot balancing.

B. EXPERIMENTAL RESULTS

The Single Support Phase (SSP) and the Double Support Phase (DSP) situations during force measurements are schematically explained in Fig. 3. When the robot is standing on the inclined surface, supported on both feet, the robot is said to be in the DSP. Otherwise, when the robot lifts one leg for walking and is solely supported by the other leg, the robot is considered to be in the SSP of the walking. The SSP stability is the major concern of the present investigation. Fig. 4(a) gives an example of the measured time-dependent toe and heel forces at the left leg on a 3.8°-inclined surface, when the right leg goes through the process of lifting, then being stably lifted and afterwards touching down again onto the surface. Fig. 4(b) shows the time-dependent toe- and heel-force data at the left leg for different inclinations during the SSP with the right leg lifted. The downslope surface-inclination angles of 2.7°, 3.8° and 5.3° are identified by the different symbols. With increased inclination, the detected forces on toe and heel are further split apart. Fig. 5 shows the summarized toe- and heel-force measurements under the equilibrium conditions as a function of surface inclination ϕ (a) for left leg and (b) for right leg. The values are those at the time shown by the black arrow in Fig. 4(a), at the SSP end. Since the robot is not completely symmetrical, the measured forces at left and right leg are not completely identical. It is further observed, that the toe force increases while the heel force decreases

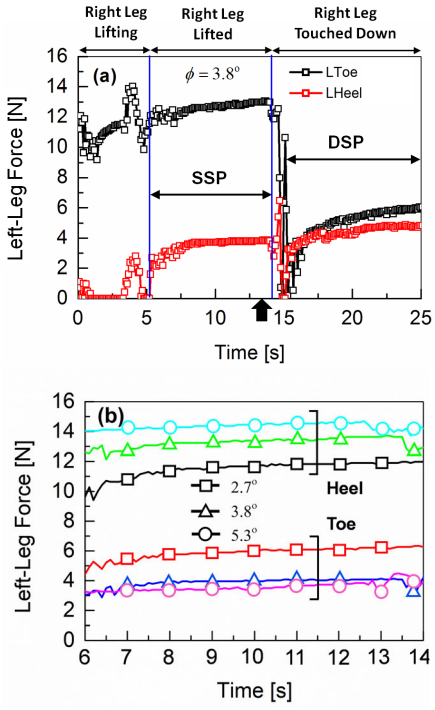

FIGURE 4. (a) Example for the time-dependent measurements of heel and toe forces at the left leg, during a lifting cycle of the right leg on a 3.8° inclined surface. The black arrow indicates our measurement-time point for the force. (b) Measurement data of toe and heel forces at the left leg for different surface inclinations under the SSP condition.

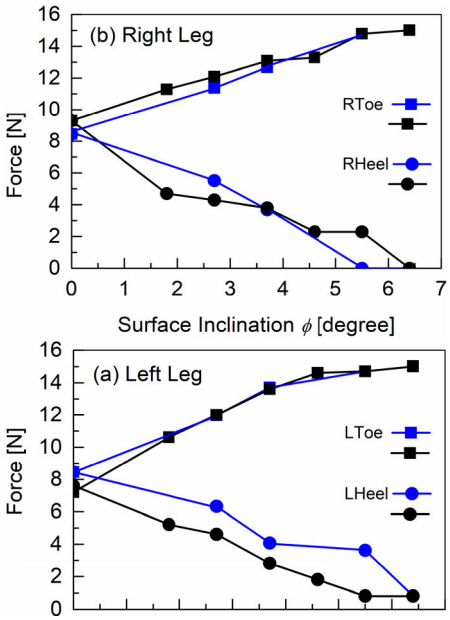

FIGURE 5. Force-sensor measured toe and heel forces of the robot for (a) left and (b) right leg at the end of the SSP, as indicated with a black arrow in Fig.4(a). Two measurement data for identical conditions are depicted together, to show the measurement variation due to differences in the robot's balancing condition.

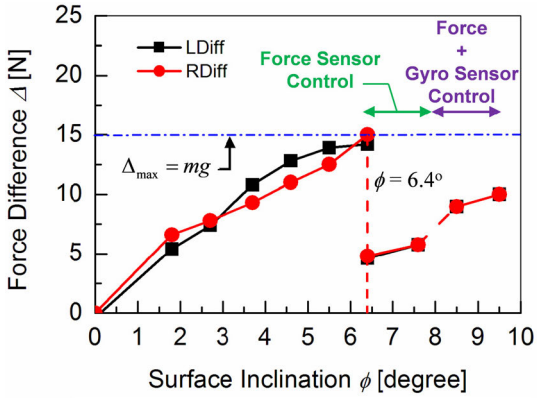

FIGURE 6. Force-difference plots at toe and heel as a function of surface inclination, measured during the robot-walking experiments for both, the left and the right leg. Here we use following notations, LDiff: Force difference between toe and heel at left leg, RDiff: Force difference between toe and heel at right leg.

with increasing ϕ for the downslope case. Two measurement results are depicted together (see Fig. 5), to demonstrate the small observed variation due to body-posture changes. This is caused by the dynamic robot balancing, having relatively large variations in comparison to other reports, because we use a light-weight robot. It can be seen, that the robot is balanced only on the toe, i.e., the heel force is becoming zero, when the surface inclination becomes about $\phi = 6.4°$. Consequently, the robot falls forward for surface inclinations larger than $\phi = 6.4°$.

Starting from a surface inclination of $\phi = 6.4°$, measurements according to the 2nd situation are therefore performed, namely, the ankle-pitch motor (M_A) is adjusted based on the difference (Δ) between toe and heel forces of the supporting leg, so that the robot's forward falling is prevented by assuring that the whole robot foot touches the surface. Fig. 6 shows the measured force difference Δ, plotted as a function of ϕ for $\phi < 8.5°$, where only the ankle-pitch motor M_A is controlled via the robot's feedback-control system. The M_A-angle adjustment is done with an implemented Proportional-Integral-Differential (PID) control system, which moves the robot posture backwards to make the robot balanced.

Our measurements verify, that the robot can be balanced up to 7.6° of surface inclination by adjusting the ankle-pitch motor M_A. Beyond that inclination, the robot falls forward again. Therefore, the angle of the hip-pitch motor M_H is additionally adjusted, corresponding to the 3rd measurement situation. Achieved results are also depicted in Fig. 6. Now the robot can sustain a stable posture up to 9.6° surface inclination, using a two-motor control based on data from two sensor types. However, above motor control for robot-posture stabilization has led to a much smaller increase of the safely walkable surface inclination, than what we would have expected, as observed from a still relatively large Δ even after the additional control.

III. MODEL DEVELOPMENT FOR ROBOT BALANCING

Our modeling-investigation purpose is to achieve an effective utilization of the measured sensor data to balance the robot posture. The focus is mostly given on the force-sensor information, which provides the surface-inclination information.

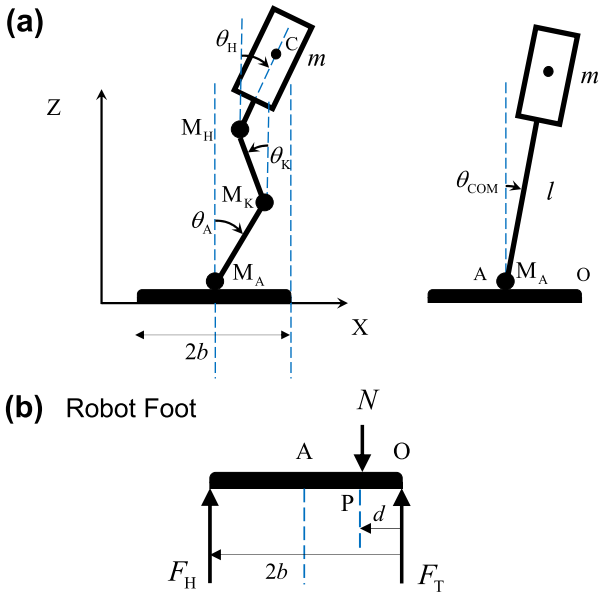

FIGURE 7. (a) Inverted pendulum model (IPM) with 3-degrees of freedom and its simplification. (b) Free-body diagram of the robot foot. The downward arrow denotes the force by the robot body and the upward arrows indicate the reaction forces, detected by the sensors.

The robot motion for a surface inclination ϕ is modeled during our analysis by extending the Inverted Pendulum Model (IPM) [43]–[45]. The extended IPM model is then used to determine the required motor adjustment for effective robot balancing.

A. IPM FOR ROBOT-FOOT-CENTRIC BALANCING

The IPM describes the robot motion with a fixed mass position, i.e., a COM description, connected by a link to a fulcrum. The robot model and its model parameters are illustrated in Fig. 7(a) [43]–[45], where l is determined experimentally by the see-saw method [48]. The variables and parameters used in the model are also listed in Table 2. For simplicity, the entire robot mass m is assumed to be concentrated at the point C of the pendulum bob, which represents the COM of the robot. The links connecting the fulcrum and the robot COM are considered to be massless. The model assumes further a massless foot of length $2b$, measured from the foot toe, where the toe is denoted by O (see Fig. 7(b)). The ankle-pitch motor M_A is the major adjustment target for reflecting and compensating the surface conditions. Thus, the two angles θ_H and θ_K are here set to be constants, so that the robot's stabilization is studied only by using the ankle-pitch-motor angle θ_A. Therefore, θ_{COM} is equal to θ_A in this case. The ankle-pitch motor is assumed to be connected to the foot at the point A, the fulcrum in the middle of the foot.

Under above simplifications, the equation of motion for the inverted pendulum can be written as [43]

$$J_A\ddot{\theta}_A = -mgl\sin\theta_A + N \times (b - d) \tag{1}$$

where $J_A(= ml^2)$ is the moment of inertia of the pendulum about the point A, and g is the earth's surface acceleration.

TABLE 2. Variables and parameters used in the inverted pendulum model (IPM).

Parameter	Symbol	Unit
Robot COM link length	l	m
Mass	m	kg
Earth's surface acceleration	g	$m{\cdot}s^{-2}$
Ankle-pitch motor	M_A	-
Knee motor	M_K	-
Hip-pitch motor	M_H	-
Ankle-pitch-motor angle	θ_A	degree
Knee-motor angle	θ_K	degree
Hip-pitch-motor angle	θ_H	degree
Center-of-Mass-position angle	θ_{COM}	degree
Foot length	$2b$	m

The first term on the right-hand side of (1) describes the torque due to the gravity, and the second term describes the torque induced to compensate this gravity torque. From (1) it can be observed, that the compensating torque for static stability of the robot is provided by the vertical ground-reaction force N against the torque due to gravity. The force N is acting on the robot foot at the point P, called the Zero Moment Point (ZMP) [46], which is considered to be at a distance d from the point O, as shown in Fig. 7(b). Since we have introduced two force sensors at toe and heel of the robot foot, the vertical ground-reaction force at each sensor position is detected and is acting vertically upward through the toe and the heel, as depicted in Fig. 7(b) by upward arrows. The forces denoted F_H and F_T are these respective vertical reaction forces, which act on heel and toe of the robot foot and are induced according to the robot's body inclination. It can be seen in Fig. 7(b), that moments are induced around toe-point O due to force N at a distance d from the toe and due to force F_H at a distance $2b$ (length of the robot feet) from the toe. By considering that the net moment around the point O should be equal to zero under the equilibrium condition, we obtain the torque-balance equation given by

$$F_H \times 2b = N \times d \tag{2}$$

and thus

$$F_T = N \times \left(\frac{2b - d}{2b}\right); \quad F_H = N \times \left(\frac{d}{2b}\right) \tag{3}$$

where $F_T + F_H = N$. The force difference Δ is defined as the difference between toe and heel reaction forces, which is written as a function of the distance d

$$\Delta = F_T - F_H = N \times \left(\frac{b - d}{b}\right) \tag{4}$$

Thus, substituting (4) into (1), the equation of motion of the inverted pendulum can be rewritten as

$$J_A\ddot{\theta}_A = -mgl\sin\theta_A + (\Delta \times b) \tag{5}$$

Consequently, the equation of motion is now written as a function of measured sensor data $\Delta = F_T$-F_H. Equation (5)

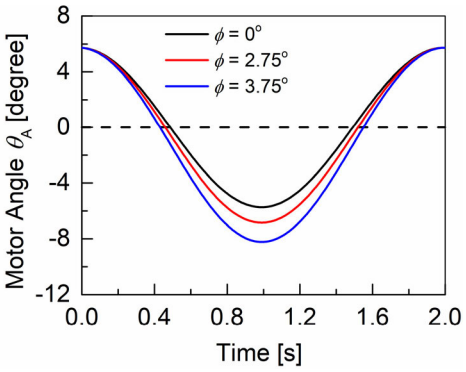

FIGURE 8. Asymmetrical shift of the oscillation of the motor angle θ_A around $\theta_A = 0$ for $\phi > 0$, due to the rotation of the robot's reference frame on the inclined surface.

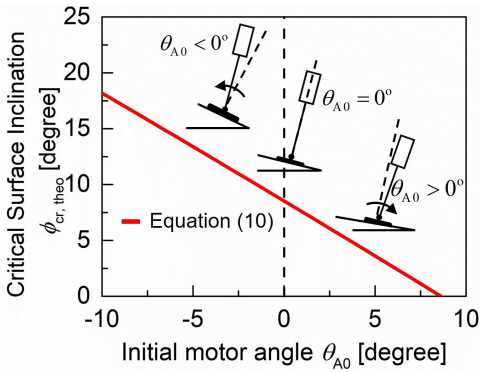

FIGURE 9. Initial angle of the robot determines the static stability margin of the robot according to the (10).

confirms, that an increase in the force difference Δ leads to the requirement of higher motor torque for compensating the torque $mgl \sin\theta_A$ induced by the gravity.

B. EXTENSION OF IPM FOR INCLIEND SURFACES

Based on the robot-balancing measurement shown in Fig. 6, modeling of the robot motion based on the IPM is extended by considering the surface inclination ϕ. Our focus is given on the SSP condition (see Fig. 3), where the robot lifts one leg without walking, thus keeping the stable static condition as considered for the measurements.

The equation of robot motion can be modelled with the IPM by considering the inclination ϕ of the surface, leading to an extension of (5) as

$$J_A\ddot{\theta}_A = -mgl\sin(\theta_A + \phi) + \Delta \times b \tag{6}$$

where the first term of the right-hand side is now modulated by the surface inclination ϕ. Fig. 8 shows numerical calculation results of (6) for different ϕ values, where ϕ is extracted for a corresponding Δ value from the measured results of Fig. 6. It can be seen, that the motor angle θ_A oscillates symmetrically around $\theta_A = 0°$ for $\phi = 0°$. However, when the surface inclination is increased (clockwise rotation) to $\phi > 0°$, the oscillation of the motor angle θ_A becomes asymmetrical, moving further into the clockwise direction. These results show, that the robot stabilization by adjusting θ_A in the opposite direction to the surface inclination makes the oscillation of the motor angle θ_A more symmetrical again.

The robot stays at rotational equilibrium below a critical inclination angle ϕ_{cr}. Under such a stable static condition, it can be assumed that the resultant torque at M_A is maintained at being equal to zero. Based on the extended IPM, the force difference Δ under static stability can thus be analytically written with (6) as

$$\Delta = \frac{mgl\sin(\theta_A + \phi)}{b} \tag{7}$$

This relationship gives the force difference Δ as a function of the surface inclination ϕ and the M_A motor's angle θ_A. The maximum theoretical Δ is equal to the weight of the robot ($= mg$). The initial value θ_{A0} can be calculated from (7) by assuming $\phi = 0°$ and using the measured value for the force difference Δ. For our studied case θ_{A0} is equal to 0.05°.

The condition for the necessity of a motor adjustment is given by the critical inclination ϕ_{cr}, which is measured to be $\phi_{cr,exp} = 6.4°$ for our studied case. The angle ϕ_{cr} determines the surface inclination up to which the falling forward of the robot is avoided. Thus, the theoretical critical inclination $\phi_{cr,theo}$ can be calculated from

$$\Delta_{max,theo} = \frac{mgl\sin(\theta_{A0} + \phi_{cr,theo})}{b} \tag{8}$$

Using $\Delta_{max,theo} = mg$ and $\theta_{A0} = 0°$, it can be seen, that $\phi_{cr,theo}$ is determined by only the robot structure as

$$\phi_{cr,theo} = \sin^{-1}\left(\frac{b}{l}\right) \tag{9}$$

A derivation considering the minimum potential energy of the inverted pendulum [44] leads to $\phi_{cr,theo} = \tan^{-1}(b/l)$, which reduces to (9) in our practical case of $(b/l) \ll 1$. For a more general analysis, (9) is extended by considering the robot's initial ankle-pitch-motor angle θ_{A0} in the formula, which leads to

$$\phi_{cr,theo} = \sin^{-1}\left(\frac{b - l\sin\theta_{A0}}{l\cos\theta_{A0}}\right) \tag{10}$$

Equation (10) describes, that the initial motor angle θ_{A0} modifies $\phi_{cr,theo}$, as shown in Fig. 9, to larger or smaller values for increased or decreased θ_{A0}, respectively.

Since the initial value of $\theta_A (= \theta_{A0})$ is known from (7), $\phi_{cr,theo}$ can be calculated with (10) for the initial condition. In our studied case, θ_{A0} and $\phi_{cr,theo}$ are determined to be equal to 0.05° and 5.7°, respectively. The calculation results are compared with the measured results in Fig. 10. It is obvious that the real measured Δ is not a linear function of ϕ, but has a weak saturating feature. Furthermore, the measured $\phi_{cr,exp}$ is equal to 6.4°, while the theoretical prediction gives a smaller $\phi_{cr,theo} = 5.7°$, for which Δ reaches its maximum. The reason for the difference in comparison to the measured value of 6.4° is attributed to the friction effect under real practical conditions, which is induced by the interaction between the robot feet and the ground surface and can be modelled by the

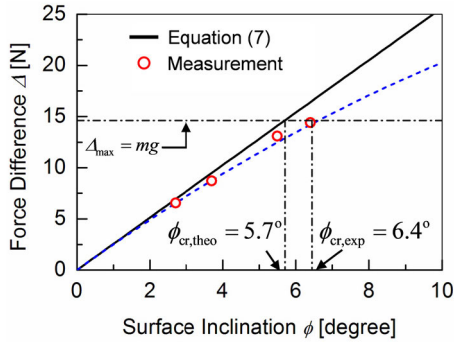

FIGURE 10. Comparison of simulated and experimentally measured force differences for both left and right leg of the robot. The cases with (dashed-blue line) and without (black-continuous line) considering the surface friction are shown.

equivalent circuit method [49], [50]. In our theoretical investigation, the surface-condition contribution for robot balancing has been neglected, and the measurements are performed for relatively slippery surfaces, i.e. surfaces with less friction.

When the surface inclination is increased beyond $\phi_{\rm cr}$, the robot falls forward. Therefore, to stabilize the robot beyond that critical inclination, the ankle-pitch-motor angle $\theta_{\rm A0}$ must be controlled first.

C. ROBOT-POSTURE CONTROL BY ANKLE-TORQUE COMPENSATION

The compensating torque of the motor was defined in the inverted pendulum's equation of motion as a function of the force-difference Δ (see (6)). Here, our focus is given on how this compensation is done, when the robot detects a change of the surface condition. Since the inclination angle ϕ cannot be measured beyond $\phi_{\rm cr}$ by using the force sensors, gyro-sensor measurements are applied for this purpose.

In our experiments, the dynamic adjustment of the angle $\theta_{\rm A}$ is started beyond $\phi = \phi_{\rm cr,exp}$. The equation of robot motion (6) on an inclined surface is rewritten with inclusion of the feedback control in the form (see also [43])

$$\begin{aligned} J_{\rm A}\ddot{\theta}_{\rm A} &= -mgl\sin(\theta_{\rm A}+\phi) + K_{\rm P}(\theta_{\rm A}^{*}-\theta_{\rm A}) \\ &\quad + K_{\rm I}\int(\theta_{\rm A}^{*}-\theta_{\rm A})dt + K_{\rm D}\frac{d}{dt}(\theta_{\rm A}^{*}-\theta_{\rm A}) \quad (11) \\ &= -mgl\sin(\theta_{\rm A}+\phi) + u(t) \quad (12) \end{aligned}$$

Since the control hardware operates in the electrical domain, the physical values of motor angles and sensor-output data are transformed into equivalent voltage values. The control parameters $K_{\rm P}$, $K_{\rm I}$ and $K_{\rm D}$ in (11) are experimentally extracted from the measured motor-armature voltage as a function of the difference between feedback-potentiometer voltage (corresponding to the measured $\theta_{\rm A}$) and reference-voltage value (corresponding to the reference angle $\theta_{\rm A}^{*}$). The difference between the equivalent voltages of $\theta_{\rm A}^{*}$ and $\theta_{\rm A}$ represents an error voltage e, which controls the armature voltage $V_{\rm arm}$ of the motor to generate the necessary torque for motor movement, as shown in Fig.11(a). The armature

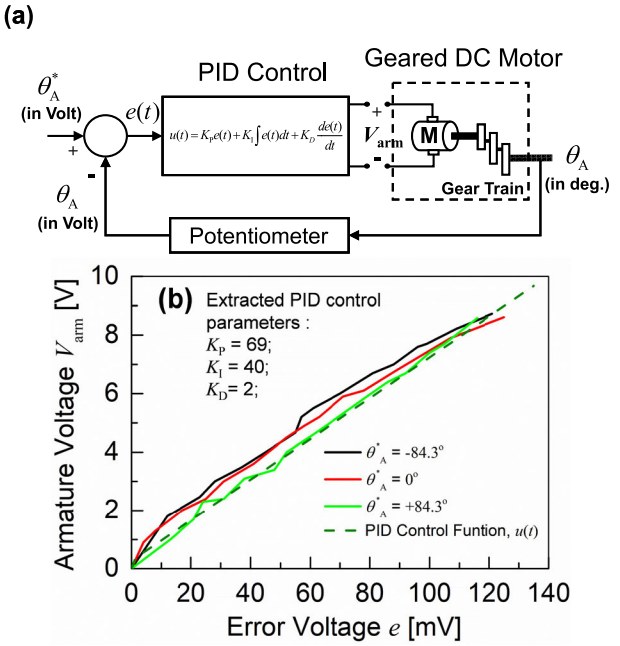

FIGURE 11. (a) Illustration of the PID control system implemented in the servomotor of the robot. (b) Measured results of armature voltage $V_{\rm arm}$ as a function of error voltage e for different reference angles $\theta_{\rm A}^{*}$ in comparison to the simulation result with the fitted PID control function. The used PDI control parameters $K_{\rm P} = 69$, $K_{\rm I} = 40$ and $K_{\rm D} = 2$ are also listed.

voltage $V_{\rm arm}$ is plotted as a function of the error voltage e for three different reference angles $\theta_{\rm A}^{*}$ (namely, $-84.3°$, $0°$ and $= +84.3°$). This relation between e and $V_{\rm arm}$ determines the PID control function $u(t)$. The fitting procedure of the control parameters $K_{\rm P}$, $K_{\rm I}$ and $K_{\rm D}$ to the experimental data resulted in their corresponding values of 69, 40 and 2, respectively, which are also listed in Fig. 11(b).

The motor angle $\theta_{\rm A}$ is rotated to $\theta_{\rm A}^{*}$ in order to keep the robot stable, namely, to suppress measured Δ below $\Delta_{\rm max}$. Fig. 12(a) shows numerical solutions of (11) under different ϕ conditions. It can be seen, that the solution converges to $\theta_{\rm A}^{*}$, when the feedback is completed. However, overshoots in $\theta_{\rm A}$ occur during this converging process to $\theta_{\rm A}^{*}$. With increased ϕ, these $\theta_{\rm A}$ overshoots become larger, which makes the robot posture increasingly unstable during the adjustment. Fig. 12(b) shows calculated torso-angular velocities ω ($= d\theta_{\rm COM}/dt$, see also Fig. 7(a)) of the robot during the feedback process together with the gyro-sensor measurements. For $\phi = 7.6°$ only $\theta_{\rm A}$ is adjusted, while an additional $\theta_{\rm H}$ rotation is done for $\phi = 9.5°$. It is confirmed, that the simplified extended-IPM-based equation of motion can predict the robot-body-adjustment process quite accurately, especially for the single-motor control ($\phi = 7.6°$ case). The observed deviations for $\phi = 9.5°$ are mostly caused by the additional $\theta_{\rm H}$ control, since the single equation of motion (11) does not describe the two independent control features. Nevertheless, agreement is basically satisfactory. The prediction, that a larger ϕ induces a larger overshoot in the angular robot-torso velocity ω, is confirmed by the measurements as well.

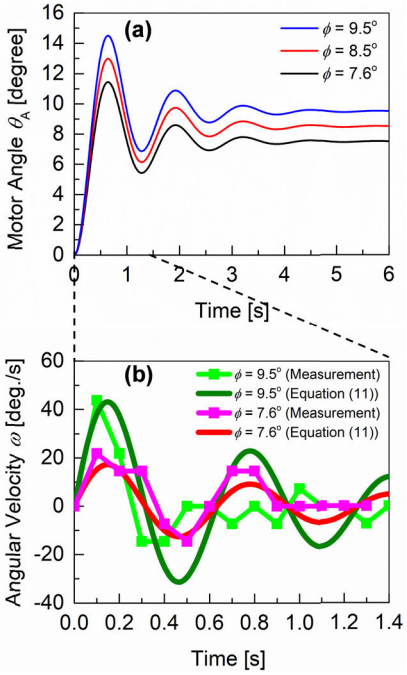

FIGURE 12. (a) Illustration of the simulated adjustment of the ankle-pitch-motor angle θ_A according to (11), when the surface inclination ϕ is increased. (b) Simulation result for the torso-angular velocity ω of the robot in comparison to the gyro-sensor measurements.

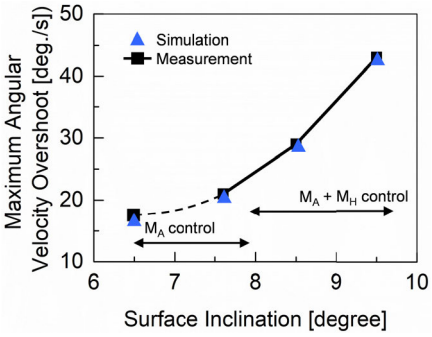

FIGURE 13. Simulation result for the maximum overshoot of the torso-angular velocity of the robot as a function of the surface inclination in comparison to the gyro-sensor measurements.

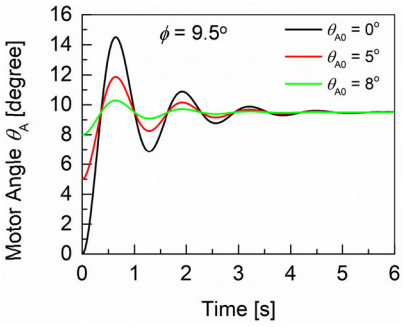

FIGURE 14. Confirmation of a drastically diminishing θ_A overshoot when the initial angle θ_{A0} is set closer to the desired value θ_A^*.

Equation (11) is derived by simplifying the robot motion, considering only the surface inclination ϕ and an adjustment of the ankle-pitch-motor angle θ_A. On the other hand, measured ω for $\phi = 9.5°$, shown in Fig. 12(b), includes an additional θ_H control. It can be seen that the measurements show a more rapid convergence of ω to zero than the simulated prediction. θ_A and θ_H are rotated in opposite directions, which is the reason for the more rapid convergence of ω to its final value. Fig. 13 compares the calculated and measured results for the maximum ω-overshoot values as a function of ϕ. A drastic increase of ω is observed for $\phi > 7.6°$, resulting from the necessity for a more rapid robot reaction to achieve posture stabilization under higher inclination conditions.

To realize a feedback control for faster robot-posture stabilization, reduction of the observed overshoots is a prerequisite. Fig. 14 shows the calculation results when the initial $\theta_A (= \theta_{A0})$ is set closer to θ_A^*, namely, the solution of equation (11). It can be seen, that such a θ_{A0} adjustment diminishes the overshoot drastically, and thus supports the robot balancing on an inclined surface, as observed also in a ϕ_{cr} increase (see Fig. 9). When the robot-posture correction is completed, the second term on the right side of (11) reduces to zero. This means θ_A becomes equal to θ_A^* as well as to ϕ. Above relationship can be utilized by using the ϕ extracted from the measured Δ value for rotating θ_{A0} close to θ_A^*, before starting the conventional feedback control. In this way the surface inclination, calculated immediately from the measured force-sensor data, can help to improve the robot-posture stability. As mentioned before, equation (11) is simplified by considering just the surface inclination ϕ. However, θ_A^* cannot be expected to become exactly equal to ϕ, because other contributions exist in a real system. To obtain better knowledge of the accurate θ_A^* value is a major target for further improvements.

IV. ANALYSIS OF MEASURED CONTROL FEATURES

In Fig. 6, we have plotted the measured Δ as a function of the inclination angle ϕ. The robot-motor control is done by implementing two additional equations of motion into the robot system, which are activated at surface inclinations $\phi \geq \phi_{cr,exp}$ and use measured data for Δ and ω. The implementation is done according to the schematic diagram of Fig. 15. Two online streams of measured data are treated independently with independent equations of motion, and the Kondo robot merges them into its unified system, containing also many other motors. The equation of motion is often much more complicated than the one we have adopted in (11).

In the electrical feedback controlling of the robot, most effort is given on obtaining an appropriate solution θ_A^* (and also θ_H^*). The measured data (Δ and ω) are integrated into the robot system for determining θ_A^* in the form

$$\theta_A^* = \theta_{A,0} + K_A \Delta \quad (13)$$

$$\theta_H^* = \theta_{H,0} + K_H(\omega_{ref} - \omega_{meas}) \quad (14)$$

where ω_{meas} and ω_{ref} are measurements and reference value of the angular robot-torso velocity, respectively. The reference value ω_{ref} for the angular robot-torso velocity is set equal to 0 deg/s. K_A and K_H are adjustable parameters including the

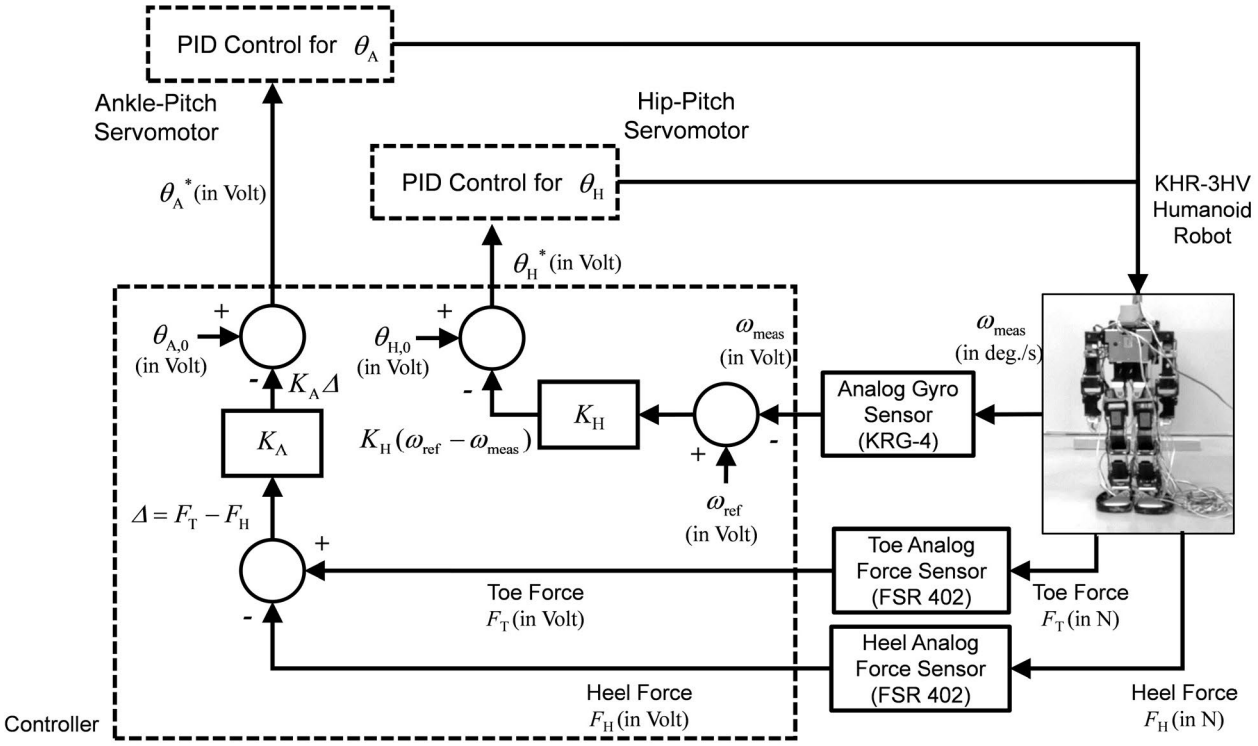

FIGURE 15. Schematic diagram of the implemented control system for the ankle-pitch-motor angle θ_A and the hip-pitch-motor angle θ_H.

dimension transformation, which quantify the stiffness [51] between the motor and its load. For higher compensating torque, needed to stabilize the robot-posture, higher K_A and K_H values are required. The lower limit of K_A and K_H is adjusted so that the force difference between toe and heel of the robot becomes minimum, while ankle- and hip-motor torque remain sufficient to make the robot posture stable. Therefore, we set the K_A value to 12, so that the most stable condition and minimum Δ for $\phi = 6.4°$ are realized. Based on the θ_A control, the measured Δ reduction is substantial (i.e., toe and heel are more balanced), and thus the robot is able to keep a stable posture up to 7.6° surface inclination. Due to the θ_A rotation (i.e., the setting of a new θ_{A0}), the critical surface inclination ϕ_{cr} should in principle increase according to the theoretical data shown in Fig. 9. However, it is found experimentally, that the robot falls down at much smaller surface inclinations ϕ than the expected $\phi_{cr,theo}$. The reason could be the relatively slippery condition of robot feet and applied surface. Figure 16 adds a measurement extension with increased K_A to the plot shown in Fig. 6. With the increase in the surface inclination, a higher K_A value is required to increase the torque at the ankle-pitch motor for robot stabilization. But K_A cannot be increased beyond a limit, as this would cause instabilities in the robot due to vibrations. Consequently, based on the trade-off between a sufficient torque to control the robot motors and the degree of robot vibrations, the value of K_A is optimized and implemented in the control system. As observed in our experiment, the robot can thus maintain a stable condition up to $\phi = 8.88°$, as plotted in Fig. 16 for $K_A = 14$. Therefore, K_A–adjustment according to the ϕ increase is a viable solution for achieving stable robot posture under situations with changing surface inclinations. To further increase the robot stability, an increase of K_H is also investigated. Following the same process as discussed before, it is found to enable robot-body stability up to 10.2° of surface inclination.

As can be seen in Fig. 16, an additional θ_H control is undertaken beyond $\phi = 7.6°$. As an unexpected result, the Δ value increases to a higher level than during the single-motor control of θ_A, as depicted in Fig. 16 by an upward arrow. The reason for this Δ increase, rather than the expected reduction, can be attributed to the fact, that the rotations for θ_A and θ_H are done in opposite directions, which induces also a length reduction of the inverted pendulum and is known to increase the postural robot stability even on flat surfaces [45].

The hip-motor angle θ_H is calculated from the inverse kinematics [25] of the robot, considering an IPM with 2 degrees of freedom. The hip-motor position is approximated to be in the middle of the inverted-pendulum length l for the IPM with 1 degree of freedom.

$$\theta_H = 2\theta_{COM} - 2\theta_A \tag{15}$$

Here, the ankle-pitch-motor angle θ_A is the calculated value by extrapolating the ankle-motor-control strategy, as indicated in Fig. 16 by the lower dashed line, while the Δ value is calculated using (7). Assuming that the θ_A rotation is the same for both control methods, the calculated values with (15) are used for θ_H determination. θ_{COM} is calculated from (7) by extrapolating the force- and gyro-sensor control strategy. The determined values for θ_H, θ_A and θ_{COM} are shown in Fig. 17

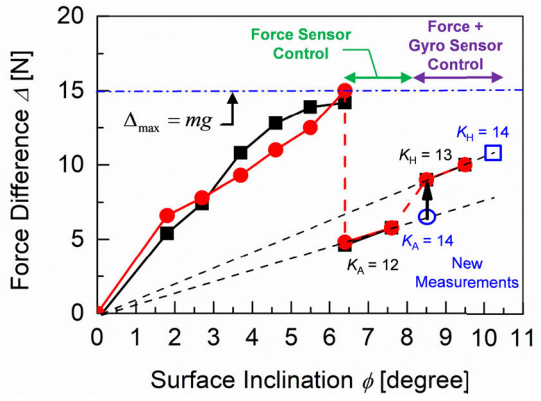

FIGURE 16. Extended robot-stability results for higher surface inclinations due to adjustment of feedback-control parameters (see (12) and (13)).

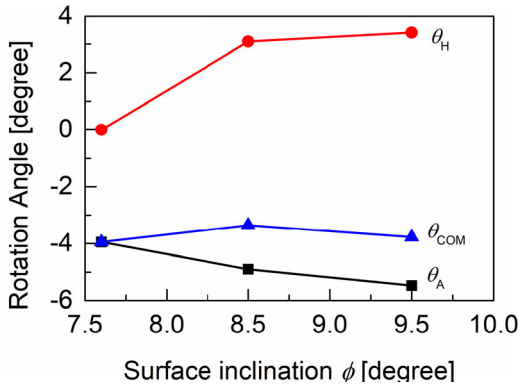

FIGURE 17. Adjustment of the robot's center of mass (COM) angle θ_{COM} as a function of surface inclination ϕ, due to feedback control of ankle-pitch-motor angle θ_A and hip-pitch-motor angle θ_H.

as a function of the surface inclination ϕ. It can be seen, that above a surface inclination of 7.6°, the hip-motor angle θ_H rotation is about twice as large as for the ankle-pitch-motor angle θ_A, while θ_{COM} stays nearly constant. This means, that the hip-motor control is mainly responsible for the robot-posture stabilization in the area of larger surface inclinations.

Figure 12(b) has compared in particular the measured ω as a function of time for two different surface inclinations, namely, one with a single-motor-control scheme and the other with a two-motor-control scheme. Interestingly, maximum ω increases with increased ϕ, indicating higher motor velocity for such steeper surface inclinations. This means, that quicker reactions of the robot are required on further inclined surfaces, to avoid the robot's down falling. Consequently, it can be concluded that not only the motor angle but also the adjustment speed must be controlled at the same time. We found that this can be done exploiting the ω measurement of a gyro-sensor, allowing the adjustment-speed optimization as a function of the surface inclination ϕ.

V. CONCLUSION AND FUTURE WORK

Our focus has been given on the robot-stability maintenance on inclined surfaces, by investigating the robot motion on such inclined surfaces experimentally as well as theoretically. The surface-inclination angle ϕ is shown to be determinable from the difference Δ of the measured responses from two force sensors, attached to toe and heel of each robot foot. Our measurements reveal that the robot requires no feedback control up to a critical surface inclination ϕ_{cr}. This measured result is modeled simply as a function of the robot size, which is extended to include the robot's posture feature.

For surface inclinations beyond ϕ_{cr}, an electrical feedback control of the ankle-pitch motor is introduced to sustain the surface connection of the robot feet, meaning that the force difference Δ between toe and heel of the robot feet is reduced to a smaller value than its maximum, which allows the robot to keep a stable posture. When the surface inclination is increased further, however, the ankle-pitch-motor control alone is no longer able to maintain the stable robot posture. Therefore, a gyro-sensor-based hip-motor adjustment is additionally introduced into the control system.

Further, the Inverted Pendulum Model (IPM) is extended to include the surface-inclination effect on the robot motion, under which the robot has to keep its stable posture. It is shown, that this extended IPM can accurately reproduce gyro-sensor-measured angular velocities during feedback control on inclined surfaces. However, the feedback control itself can also cause robot instability. To improve this situation, we demonstrated that sensor-detected environmental changes are better utilized immediately to stabilize the robot posture by an initial motor rotation, thus bypassing the normal feedback control. It is verified with the extended IPM, that the derived relation between measured force difference Δ and surface inclination ϕ can also be used for executing such an initial rotation of the ankle-pitch-motor angle θ_A.

Usually, the Zero Moment Point (ZMP) is used to characterize robot instabilities on inclined surfaces. However, our developed method for using the measured force differences Δ at toe and heel of the robot feet as the core measure for robot-instability characterization provides a simpler and yet accurate approach.

In this work a relatively slippery surface has been considered. A remaining task, which we plan to investigate in more detail in our future work, is the general effect of friction between the robot feet and the surface, which is expected to be quite crucial for the walking of a humanoid robot on an inclined surface. Lower surface friction will most likely limit the critical surface inclination ϕ_{cr} as a function of the surface inclination ϕ, as indicated in Fig. 10. Therefore, it will be important to incorporate the surface-friction effects into a further extended IPM, to enable in particular a more accurate prediction of the critical surface inclination as well as improved predictions of the reference values for the motor-angle-adjustment control (e.g. a more accurate θ_A^* value for the ankle-motor-angle control).

Another envisaged future work is an extension of the present control system to dynamic robot walking on surfaces with increased roughness, where we expect that the real-time information from force and gyro sensors will also be very helpful for improving the dynamic stability of humanoid robots.

REFERENCES

[1] F. A. Auat Cheein and R. Carelli, "Agricultural robotics: Unmanned robotic service units in agricultural tasks," *IEEE Ind. Electron. Mag.*, vol. 7, no. 3, pp. 48–58, Sep. 2013.

[2] C. Heyer, "Human-robot interaction and future industrial robotics applications," in *Proc. IEEE/RSJ Int. Conf. Intell. Robots Syst.*, Taipei, Taiwan, Oct. 2010, pp. 4749–4754.

[3] J. Casper and R. R. Murphy, "Human-robot interactions during the robot-assisted urban search and rescue response at the world trade center," *IEEE Trans. Syst., Man, Cybern., B (Cybern.)*, vol. 33, no. 3, pp. 367–385, Jun. 2003.

[4] M. Burri, J. Nikolic, C. Hurzeler, G. Caprari, and R. Siegwart, "Aerial service robots for visual inspection of thermal power plant boiler systems," in *Proc. 2nd Int. Conf. Appl. Robot. for Power Ind. (CARPI)*, Zurich, Switzerland, Sep. 2012, pp. 70–75.

[5] T. Yoshida, K. Nagatani, S. Tadokoro, T. Nishimura, and E. Koyanagi, "Improvements to the rescue robot quince toward future indoor surveillance missions in the Fukushima Daiichi nuclear power plant," in *Field and Service Robotics. Springer Tracts in Advanced Robotics*, K. Yoshida and S. Tadokoro, Eds. Berlin, Germany: Springer, 2014.

[6] B. Kuipers and Y.-T. Byun, "A robot exploration and mapping strategy based on a semantic hierarchy of spatial representations," *Robot. Auto. Syst.*, vol. 8, nos. 1–2, pp. 47–63, Nov. 1991.

[7] A. Hornung, K. M. Wurm, and M. Bennewitz, "Humanoid robot localization in complex indoor environments," in *Proc. IEEE/RSJ Int. Conf. Intell. Robots Syst.*, Taipei, Taiwan, Oct. 2010, pp. 1690–1695.

[8] S. Kuindersma, R. Deits, M. Fallon, A. Valenzuela, H. Dai, F. Permenter, T. Koolen, P. Marion, and R. Tedrake, "Optimization-based locomotion planning, estimation, and control design for the atlas humanoid robot," *Auto. Robots*, vol. 40, no. 3, pp. 429–455, Mar. 2016.

[9] H. Dai and R. Tedrake, "Planning robust walking motion on uneven terrain via convex optimization," in *Proc. IEEE-RAS 16th Int. Conf. Humanoid Robots (Humanoids)*, Cancun, Mexico, Nov. 2016, pp. 579–586.

[10] A. Hereid, E. A. Cousineau, C. M. Hubicki, and A. D. Ames, "3D dynamic walking with underactuated humanoid robots: A direct collocation framework for optimizing hybrid zero dynamics," in *Proc. IEEE Int. Conf. Robot. Autom. (ICRA)*, Stockholm, Sweden, May 2016, pp. 1447–1454.

[11] M. Morisawa, S. Kajita, F. Kanehiro, K. Kaneko, K. Miura, and K. Yokoi, "Balance control based on capture point error compensation for biped walking on uneven terrain," in *Proc. 12th IEEE-RAS Int. Conf. Humanoid Robots (Humanoids)*, Osaka, Japan, Nov. 2012, pp. 734–740.

[12] C. Chew, J. Pratt, and G. Pratt, "Blind walking of a planar bipedal robot on sloped terrain," in *Proc. IEEE Int. Conf. Robot. Automat.*, Kyongju, South Korea, May 1999, pp. 381–386.

[13] Y. Hidaka, K. Nishizawa, and D. N. Nenchev, "Dynamic stepping on unknown obstacles with upper-body compliance and angular momentum damping from the reaction null-space," in *Proc. Int. Conf. Robot. Autom. (ICRA)*, Montreal, QC, Canada, May 2019, pp. 5273–5279.

[14] Q. Nguyen, A. Agrawal, W. Martin, H. Geyer, and K. Sreenath, "Dynamic bipedal locomotion over stochastic discrete terrain," *Int. J. Robot. Res.*, vol. 37, nos. 13–14, pp. 1537–1553, Dec. 2018.

[15] G. Nelson, A. Saunders, and R. Playter, "The PETMAN and atlas robotsat Boston dynamics," in *Humanoid Robotics: A Reference*. Berlin, Germany: Springer, 2019, pp. 169–186.

[16] Q. Li, Z. Yu, X. Chen, Q. Zhou, W. Zhang, L. Meng, and Q. Huang, "Contact force/torque control based on viscoelastic model for stable bipedal walking on indefinite uneven terrain," *IEEE Trans. Automat. Sci. Eng.*, vol. 16, no. 4, pp. 1627–1639, Oct. 2019.

[17] F. Segulla and D. Rixen, "A force-control scheme for biped robots to walk over uneven terrain including partial footholds," *Int. J. Adv. Robotic Syst.*, vol. 17, no. 1, pp. 1–14, Jan. 2020.

[18] M. Favre, B. Goodwine, and J. P. Schmiedeler, "Terrain-blind walking of planar underactuated bipeds via velocity decomposition-enhanced control," *Int. J. Robot. Res.*, vol. 38, nos. 10–11, pp. 1307–1323, Aug. 2019.

[19] D. Wahrmann, A. C. Hilderbrandt, and T. Bates, "Vision-based 3D modeling of unknown dynamic environments for real-time humanoid navigation," *Int. J. Humanoid Robot.*, vol. 16, no. 1, 2019, Art. no. 1950002.

[20] A.-C. Hildebrandt, R. Wittmann, F. Sygulla, D. Wahrmann, D. Rixen, and T. Buschmann, "Versatile and robust bipedal walking in unknown environments: real-time collision avoidance and disturbance rejection," *Auto. Robots*, vol. 43, no. 8, pp. 1957–1976, Dec. 2019.

[21] S. Kajita, F. Kanehiro, K. Kaneko, K. Yokoi, and H. Hirukawa, "The 3D linear inverted pendulum mode: A simple modeling for a biped walking pattern generation," in *Proc. IEEE/RSJ Int. Conf. Intell. Robots Syst. Expanding Societal Role Robot. Next Millennium*, Maui, HI, USA, Oct./Nov. 2001, pp. 239–246.

[22] T. McGeer, "Passive dynamic walking," *Int. J. Robot. Res.*, vol. 9, no. 2, pp. 62–82, Apr. 1990.

[23] S. H. Collins, M. Wisse, and A. Ruina, "A three-dimensional passive-dynamic walking robot with two legs and knees," *Int. J. Robot. Res.*, vol. 20, no. 7, pp. 607–615, Jul. 2001.

[24] J. Chestnutt, M. Lau, G. Cheung, J. Kuffner, J. Hodgins, and T. Kanade, "Footstep planning for the honda ASIMO humanoid," in *Proc. IEEE Int. Conf. Robot. Autom.*, Barcelona, Spain, Apr. 2005, pp. 629–634.

[25] S. Kajita, H. Hirukawa, K. Harada, and K. Yokoi, *Introduction to Humanoid Robotics*. Berlin, Germany: Springer-Verlag, 2014, pp. 45–65, 69-97.

[26] M. Vukobratovic and B. Borovac, "Zero-moment point—Thirty five years of its life," *Int. J. Humanoid Robot.*, vol. 1, no. 1, pp. 157–173, 2004.

[27] *ASIMO Technical Information*, Honda Motor Co., Ltd., Shizuoka, Japan, 2007.

[28] K. Kaneko, F. Kanehiro, M. Morisawa, T. Tsuji, K. Miura, S. Nakaoka, S. Kajita, and K. Yokoi, "Hardware improvement of cybernetic human HRP-4C for entertainment use," in *Proc. IEEE/RSJ Int. Conf. Intell. Robots Syst.*, CA, USA, Sep. 2011, pp. 4392–4399.

[29] *Development of a Humanoid Robot Prototype, HRP-5P, Capable of Heavy Labor*, National Institute of Advanced Industrial Science and Technology (AIST), Tokyo, Japan, Nov. 2018.

[30] K. C. Lau, "A flexible surgical robotic system for removal of early-stage gastrointestinal cancers by endoscopic submucosal dissection," *IEEE Trans. Ind. Informat.*, vol. 12, no. 6, pp. 2365–2374, Dec. 2016.

[31] Z. Zhang, L. Zheng, Z. Chen, L. Kong, and H. R. Karimi, "Mutual-Collision-Avoidance scheme synthesized by neural networks for dual redundant robot manipulators executing cooperative tasks," *IEEE Trans. Neural Netw. Learn. Syst.*, early access, Apr. 20, 2020, doi: 10.1109/TNNLS.2020.2980038.

[32] J.-G. Juang, "Locomotion control using environment information inputs," in *Proc. Int. Conf. Inf. Intell. Syst.*, Bethesda, MD, USA, Oct./Nov. 1999, pp. 196–201.

[33] J. P. Ferreira, M. Crisostomo, A. P. Coimbra, and B. Ribeiro, "Simulation control of a biped robot with support vector regression," in *Proc. IEEE Int. Symp. Intell. Signal Process.*, Xiamen, China, Oct. 2007, pp. 1–6.

[34] X. Da, R. Hartley, and J. W. Grizzle, "Supervised learning for stabilizing underactuated bipedal robot locomotion, with outdoor experiments on the wave field," in *Proc. IEEE Int. Conf. Robot. Autom. (ICRA)*, Singapore, May 2017, pp. 3476–3483.

[35] A. W. Salatian, K. Y. Yi, and Y. F. Zheng, "Reinforcement learning for a biped robot to climb sloping surfaces," *J. Robotic Syst.*, vol. 14, no. 4, pp. 283–296, Apr. 1997.

[36] G. Endo, J. Morimoto, T. Matsubara, J. Nakanishi, and G. Cheng, "Learning CPG-based biped locomotion with a policy gradient method: Application to a humanoid robot," *Int. J. Robot. Res.*, vol. 27, no. 2, pp. 213–228, Feb. 2008.

[37] S. Kajita and K. Tani, "Study of dynamic biped locomotion on rugged terrain-derivation and application of the linear inverted pendulum mode," in *Proc. IEEE Int. Conf. Robot. Autom.*, Sacramento, CA, USA, Apr. 1991, pp. 1405–1411.

[38] S. G. Tzafestas, T. E, Krikochoritis and C. S. Tzafestas, "Robust sliding-mode control of nine-link biped robot walking," *J. Intell. Robot. Syst.*, vol. 20, nos. 2–4, pp. 375–402, Sep. 1997.

[39] H. V. D. Kooij, R. Jacobs, B. Koopman, and F. V. D. Helm, "An alternative approach to synthesizing bipedal walking," *Biol. Cybern.*, vol. 88, no. 1, pp. 46–59, Jan. 2003.

[40] D. Toricelli, "Benchmarking human likeness of bipedal robot locomotion: State of the art and future trends," in *Metrics of Sensory Motor Coordination and Integration in Robots and Animals* (Cognitive Systems Monographs), vol. 36. F. Bonsignorio, E. Messina, A. del Pobil, and J. Hallam, Eds. Cham, Switzerland: Springer, 2020.

[41] K. Tamura and A. Kawamura, "Robust and high-mobility walking control for uneven terrain without zero-moment-point feedback," in *Proc. IEEE Int. Conf. Ind. Technol. (ICIT)*, Toronto, ON, Canada, Mar. 2017, pp. 866–871.

[42] S. Yi, B. Zhang, and D. D. Lee, "Online Learning of Uneven Terrain for Humanoid Bipedal Walking," in *Proc. AAAI Conf. Artif. Intell. (AAAI)*, Atlanta, GA, USA, 2010, pp. 1639–1644.

[43] H. Hemami and C. L. Golliday, "The inverted pendulum and biped stability," *Math. Biosci.*, vol. 34, nos. 1–2, pp. 95–110, Jan. 1977.
[44] H. Hemami, F. C. Weimer, and S. H. Koozekanani, "Some aspects of the inverted pendulum problem for modeling of locomotion systems," *IEEE Trans. Autom. Control*, vol. 18, no. 6, pp. 658–661, Dec. 1973.
[45] R. B. McGhee and M. B. Kuhner, "On the dynamic stability of legged locomotion systems," in *Proc. 3rd Int. Symp. External Control Human Extremities*, Dubrovnik, Yugoslovia, 1969, pp. 431–442.
[46] M. Vukobratovic, A. A. Frank, and D. Juricic, "On the stability of biped locomotion," *IEEE Trans. Biomed. Eng.*, vol. BME-17, no. 1, pp. 25–36, Jan. 1970.
[47] S. Kajita and K. Tani, "Experimental study of biped dynamic walking," *IEEE Control Syst.*, vol. 16, no. 1, pp. 13–19, Feb. 1996.
[48] *KHR-3HV Humanoid Robot*, Kondo Kagaku Co. Ltd., Tokyo, Japan, 2019. [Online]. Available: http://kondo-robot.com
[49] T. K. Maiti, L. Chen, H. Zenitani, H. Miyamoto, M. Miura-Mattausch, and H. J. Mattausch, "Compact Electro-Mechanical-Fluidic model for actuated fluid flow system," *IEEE J. Multiscale Multiphys. Comput. Techn.*, vol. 2, pp. 124–133, 2017.
[50] T. K. Maiti, L. Chen, M. Miura-Mattausch, S. K. Koul, and H. J. Mattausch, "Physics based system simulation for robot electro-mechanical control design," in *Proc. IEEE Electron Devices Technol. Manuf. Conf. (EDTM)*, Toyama, Japan, Feb. 2017, pp. 259–261.
[51] G. Ellis, *Control System Design Guide*. Waltham, MA, USA: Butterworth-Heinemann, 2012, pp. 351–370.

SUNANDAN DUTTA received the M.Tech. degree from the Indian Institute of Engineering Science and Technology (IIEST), Shibpur, India, in 2017. He is currently pursuing the Ph.D. degree with the Graduate School of Engineering, Hiroshima University, Japan.

His research interests include legged locomotion and motion-control system for humanoid robots.

TAPAS KUMAR MAITI (Member, IEEE) received the Ph.D. degree in engineering from Jadavpur University, Kolkata, India, in 2009. He was a Postdoctoral Researcher with McMaster University, Hamilton, ON, Canada, for two years. He spent three years as a Researcher and two years as an Assistant Professor with Hiroshima University, Hiroshima, Japan, where he has been an Associate Professor since 2017.

MITIKO MIURA-MATTAUSCH (Fellow, IEEE) received the D.Sc. degree from Hiroshima University, Hiroshima, Japan.

Since 1996, she has been a Professor with Hiroshima University, where she has been leading the Ultra-Scaled Device Laboratory.

YOSHIHIRO OCHI received the B.Eng. degree from Tottori University, Tottori, Japan, in 2003.

Since 2009, he has been with Technical Center, Hiroshima University, Japan, where he is currently involved in technical support of the information systems.

NAOTO YORINO (Senior Member, IEEE) received the B.S., M.S., and Ph.D. degrees in electrical engineering from Waseda University, Japan, in 1981, 1983, and 1987, respectively. He joined Research and Development section Fuji Electric Company, Japan, from 1983 to 1984. Since 1987, he has been with Hiroshima University, where he is a Professor since 2005, the Vice Dean from 2009 to 2017. He was a Visiting Professor with McGill University, Montreal, QC, Canada, from 1991 to 1992, also a Visiting Professor with Hohai University, China, from 2014 to 2017. His activity includes the Vice President, Power, and Energy Society, IEE of Japan, from 2009 to 2011, a Neutral Member of the Rulemaking Committee, ESCJ, from 2007 to 2015, a Steering Committee Member of Japan Power Academy from 2012 to 2014, the Board of Director in iREP since 2007, and the Board of Director in IEIE of Japan since 2013. He has authored or coauthored more than 130 transaction articles in power and energy area.

HANS JÜRGEN MATTAUSCH (Senior Member, IEEE) received the Ph.D. degree from Stuttgart University, Stuttgart, Germany.

Since 1996, he has been a Professor with Hiroshima University, Hiroshima, Japan, where he has been involved in research on very large scale integration design, nano-electronics, and compact modeling.